Low barriers to internal rotation in the microwave spectrum of 2,5-dimethylfluorobenzene

Haoyue Sun, Safa Khemissi, Isabelle Kleiner, Ha Vinh Lam Nguyen

Low barriers to internal rotation in the microwave spectrum of 2,5-dimethylfluorobenzene

Haoyue Sun,[1,†] Safa Khemissi,[2,†,*] Isabelle Kleiner,[1] and Ha Vinh Lam Nguyen[2,3,*]

J. Chem. Phys. 160, 094302 (2024) ; https://doi.org/10.1063/5.0185005

[1] *Université Paris Cité and Univ Paris Est Créteil, CNRS, LISA, F-75013 Paris, France*

[2] *Univ Paris Est Créteil and Université Paris Cité, CNRS, LISA, F-94010 Créteil, France*

[3] *Institut Universitaire de France (IUF), F-75231 Paris, France*

[†] These authors contribute equally.

* Corresponding authors:

Safa Khemissi, e-mail: safa.khemissi@lisa.ipsl.fr

Ha Vinh Lam Nguyen, e-mail: lam.nguyen@lisa.ipsl.fr

We investigated the rotational spectrum of 2,5-dimethylfluorobenzene containing coupled large amplitude motions of two methyl groups in the frequency range from 2 to 26.5 GHz using a pulsed molecular jet Fourier transform microwave spectrometer. The internal rotation of two inequivalent methyl groups with low torsional barriers (around 16 cm^{-1} and 226 cm^{-1}) causes splitting of all rotational transitions into quintets with separations of hundreds of MHz between the torsional components. Spectral analysis and modeling of the observed splittings were performed using the programs *XIAM* and *BELGI-C_s-2Tops*, whereby the latter achieved measurement accuracy. The methyl internal rotation can be used to examine the electronic and steric environments around the methyl group because they affect the methyl torsional barrier. Electronic properties play a particularly important role in aromatic molecules with the presence of a π-conjugated double bond system. The experimental results were compared with those of quantum chemistry. Benchmark calculations resulted that the B3LYP-D3BJ/6-311++G(d,p) level of theory can be recommended for predicting rotational constants to guide the microwave spectral assignment of dimethylfluorobenzenes in particular and toluene derivatives in general.

I. INTRODUCTION

Large amplitude motion (LAM) is a fundamental phenomenon in physical chemistry with three prototypes: internal rotation,[1] inversion tunnelling,[2] and ring puckering.[3] Molecules undergoing internal rotation form an important and large class because this effect appears more frequently compared to the other two LAM types. The methyl group is a typical internal rotor. The internal rotation of a methyl group causes splittings of all rotational levels into an A level and a double-degenerated E level, and consequently, all rotational transitions also split into A-E doublets. The splitting pattern becomes more complicated if more than one methyl rotor are present. The

rigid-rotor model is no longer sufficient to treat the rotational spectrum in cases of LAMs. An appropriate Hamiltonian is required that takes into account the internal rotation effect and its coupling to the overall rotation of the molecule,[1] as implemented in a number of computer codes such as *XIAM*,[4] *BELGI* in the one-top[5,6] and two-top versions,[7] *RAM36*,[8] *PAM-C_{2v}-2Tops*,[9] *aixPAM*,[10] *ntop*,[11] and *ERHAM*,[12] most of them are available at the PROSPE website.[13] They all utilize in the Hamiltonian the rigid frame-rigid top model that includes centrifugal distortion terms for both the frame and the top and higher order terms for the internal rotation part; but they are different in the use of coordinates, i.e., the principal-axis method, the rho-axis method, or the combined-axis method. A short comparison can be found in Ref. [14]. Among all these code, *XIAM* is commonly used in the microwave spectroscopic community. Though the limited number of available parameters has often appeared as its drawback, especially in dealing with low-barrier internal rotations, *XIAM* can handle up to three tops, being at the same time fast and user-friendly. Many microwave spectra of a large number of molecules have been modelled with *XIAM*, varying from one-top molecules with high barriers such as acetovanillone,[15] *N*,*N*-diethylacetamide,[16] *N*-methyl-2-aminoethanol,[17] one-top molecules with intermediate barriers like 2-methylthiophene,[18] carvacrol,[19] methyl cyanoacetate,[20] one-top molecules with low barriers, i.e. 3-pentyn-1-ol,[21] 4-hexyn-3-ol,[22] 3-methylphenylacetylene,[23] to two-top molecules such as the series of 2-acetylmethylthiophene.[24-26]

For many molecules where the root-mean-square (rms) deviations of the *XIAM* fits could not achieve measurement accuracy, the program *BELGI* was applied to reduce the deviations satisfactorily by floating more higher order terms. This has been often the cases of methyl torsional barriers being lower than about 200 cm^{-1}, such as in octan-2-one,[27] allyl acetate,[28] and 2-methylthiazole.[29] Methyl acetate was the classic example showcasing the efficiency of the two-top version of *BELGI*, *BELGI-C_s-2Tops*,[7] as well as two recent examples on the 2,4-[30] and 4,5-isomers of dimethylthiazole.[31]

We recently started a systematic investigation on the isomers of dimethylfluorobenzene (DMFB), each of them undergoes two methyl internal rotations with different torsional barrier heights. The microwave spectra of the 2,3-, 2,6-, and 3,4-isomers could be well-modeled using the *XIAM* code, and the barriers to internal rotation are 216 cm^{-1} and 489 cm^{-1} for 23DMFB,[32] 237 cm^{-1} for 26DMFB,[33] as well as 456 cm^{-1} and 490 cm^{-1} for 34DMFB.[34] For the 25DMFB isomer targeted in this work, the internal rotation of the methyl group at the 2-position of the aromatic ring next to the fluorine atom features the same barrier height as that of the 2-methyl group in 23DMFB and 26DMFB, and modelling the splittings arising from this LAM was straightforward with *XIAM*. The internal rotation of the 5-methyl group with a very low barrier height of less than 20 cm^{-1}, on the other hand,

was extremely challenging. Assignment of rotational lines had to be carefully checked, and the use of *BELGI-C_s-2Tops* was essential to model the microwave spectrum of 25DMFB to measurement accuracy.

The main purpose of our present work on 25DMFB is to describe the challenge of low barrier methyl internal rotation in toluene derivatives. To deal with it, we need to use (i) quantum chemical calculations to get reliable initial values for the rotational constants and barriers to start the assignment; and (ii) several internal rotation methods to assign and model the experimental spectra because this is not straightforward in cases of low methyl barriers. Once the spectrum had been assigned and modeled, (iii) we will use the experimentally deduced barriers to methyl internal rotation to make comparisons with data available in the literature as our work on 25DMFB is one of the very few studies on aromatic molecules with two methyl rotors. Furthermore, (iv) we will use the rotational constants determined from experiments for benchmarking purpose by comparing their values to those calculated at several levels of theory in order to find one that can be helpful to guide the spectral assignment of future microwave spectroscopic investigations on toluene derivatives.

II. QUANTUM CHEMICAL CALCULATIONS

A. Geometry parameters

To obtain predicted rotational constants of 25DMFB, we performed geometry optimizations using the *Gaussian 16*[35] program package at three levels of theory: B3LYP-D3BJ/6-311++G(d,p),[36-40] MP2/6-311++G(d,p),[40,41] and MP2/6-31G(d,p).[40,41] These levels have been used for the other isomers 23DMFB, 26DMFB, and 34DMFB. We systematically apply the B3LYP-D3BJ/6-311++G(d,p) and MP2/6-311++G(d,p) levels since discrepancy between these two methods is not a rare observation.[42] In the cases of toluene derivatives in particular and molecules containing an aromatic ring in general, we often also include calculations at the MP2/6-31G(d,p) level since this level yielded equilibrium rotational constants B_e that are accidentally very close to the experimental ground state rotational constants B_0 in many previous studies on such molecules that helps the spectral assignment (see also Section IV on Results and Discussion).[43-45] The molecular geometry optimized at the B3LYP-D3BJ/6-311++G(d,p) level is shown in Fig. 1. The Cartesian coordinates can be found in Table S-I in the Supplementary Materials. We also performed anharmonic frequency calculations at the same levels to acquire calculated ground state rotational constants and centrifugal distortion constants. The results are summarized in Table I. Note that the geometry optimizations were carried out intendedly without any geometry constraints. From our experiences, if the MP2/6-311++G(d,p) level yields a non-planar symmetric structure that is caused by the orientation of the methyl group(s), as in the present case of 25DMFB (see Fig. S-1 in the Supplementary Materials),

this often indicates problems in methyl internal rotation(s) (see section II.C. below). Therefore, the μ_c dipole moment components predicted at this level is very small, but non-zero.

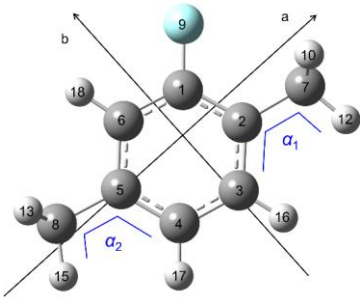

FIG. 1. Molecular geometry of 25DMFB optimized at the B3LYP-D3BJ/6-311++G(d,p) level of theory in the principal axes of inertia. The *c*-axis (not shown) is perpendicular to the *ab*-plane. The dihedral angles $\alpha_1 = \angle(C_3,C_2,C_7,H_{12})$ and $\alpha_2 = \angle(C_4,C_5,C_8,H_{15})$, describing the internal rotation of the 2- and the 5-methyl groups, respectively, are also illustrated.

TABLE I. Equilibrium rotational constants (A_e, B_e, C_e) and vibrational ground state (A_0, B_0, C_0) rotational constants, centrifugal distortion constants obtained from anharmonic frequency calculations, dipole moment components, and V_3 potentials of the two methyl groups at the 2- and 5-positions ($V_{3,2}$ and $V_{3,5}$, respectively) of 25DMFB calculated at the MP2/6-31G(d,p), MP2/6-311++G(d,p), and B3LYP-D3BJ/6-311++G(d,p) levels of theory.

Par.	Unit	MP2/ 6-31G(d,p)	MP2/ 6-311++G(d,p)	B3LYP-D3BJ/ 6-311++G(d,p)
A_e	MHz	3025.9	3012.4	3022.5
B_e	MHz	1283.9	1278.8	1285.0
C_e	MHz	911.5	907.9	911.8
A_0	MHz	3001.7	2987.2	3000.7
B_0	MHz	1276.8	1271.7	1276.9
C_0	MHz	905.9	901.9	906.0
D_J	kHz	0.02459	0.02482	0.02497
D_{JK}	kHz	0.06817	0.07435	0.13463
D_K	kHz	0.41465	0.41420	0.35009
d_J	kHz	0.00732	0.00734	0.00740
d_K	kHz	0.03622	0.04493	–0.24661
$\lvert\mu_a\rvert$	D	0.90	1.02	1.07
$\lvert\mu_b\rvert$	D	0.93	1.12	1.15
$\lvert\mu_c\rvert$	D	0.00	0.04	0.00
$V_{3,2}$	cm^{-1}	201	233	218
$V_{3,5}$	cm^{-1}	22	20	27

B. Benchmarking of the rotational constants

Benchmark calculations are more and more frequently performed in the spectroscopic community to find out the levels of theory that facilitate the assignments of microwave spectra by delivering equilibrium B_e rotational constants close to the B_0 experimental ones. From our previous benchmarking results on the 2,3-,[32] 2,6-,[33] and 3,4-isomers,[34] we continued our benchmarking efforts by utilizing a large number of method-basis set combinations to optimize the geometry of 25DMFB. The methods in use are the density functional methods B3LYP-D3,[36-38] B3LYP-D3BJ,[36-39] CAM-B3LYP-D3BJ,[46] M06-2X,[47] MN15,[48] PBE0,[49] and ωB97X-D[50] as well as the *ab initio* MP2[41] and coupled cluster CCSD[51] methods. Except for CCSD, all methods were combined with several Pople[40] and Dunning basis sets.[52] The obtained rotational constants are given in Table S-II in the Supplementary Materials.

C. Methyl internal rotations

25DMFB contains two inequivalent methyl groups undergoing internal rotation. Due to these coupled LAMs, each rotational line splits into a quintet consisting of ($\sigma_1\sigma_2$) = (00), (01), (10), (11), and (12) torsional species, where σ_1 and σ_2 refer to the 2- and the 5-methyl groups, respectively.[53] Modelling these splittings in the torsional ground state requires the V_3 potentials, sometimes also the V_6 terms and the top-top coupling terms V_{cc} and V_{ss}, to be included in the Hamiltonian in the form:

$$V(\alpha) = \frac{1}{2}\sum_{i=1}^{2}\left(V_{3,i}(1-cos3\alpha_i) + V_{6,i}(1-cos6\alpha_i)\right) + V_{cc}cos3\alpha_1 cos3\alpha_2 + V_{ss}sin3\alpha_1 sin3\alpha_2. \quad (1)$$

To obtain theoretical values for the V_3 and V_6 terms of the 2- and 5-methyl groups, potential energy curves were calculated, also at the B3LYP-D3BJ/6-311++G(d,p), MP2/6-311++G(d,p), and MP2/6-31G(d,p) levels, by altering the dihedral angles $\alpha_1 = \angle(C_3,C_2,C_7,H_{12})$ and $\alpha_2 = \angle(C_4,C_5,C_8,H_{15})$, respectively. By taking the methyl C_3 symmetry into account, only 13 steps of 10° were needed to model a full rotation. All other geometry parameters like bond angles and bond lengths were optimized. The obtained energy points were parameterized with a Fourier expansion whose Fourier coefficients are given in Table S-III in the Supplementary Materials. Using the Fourier coefficients, we plotted the potential energy curves as visualized in Figs. 2 and 3. For the 2-methyl group, the V_6 term is small compared to the V_3 term (see the value of the Fourier coefficients in Table S-III). Therefore, the curves calculated at all three levels feature a three-fold potential form reflecting the methyl C_3 symmetry. The V_3 values are given in Table I. For the 5-methyl group, the V_6 term can no longer be neglected. In calculations with the MP2 method, it even dominates the V_3 term. The respective V_3/V_6 ratios are 27.2/3.2 cm^{-1}, 20.0/23.2 cm^{-1}, and 22.0/22.6 cm^{-1}. Double minima are visible in the potential curves obtained from the two MP2 calculations, and the curve obtained with the B3LYP method features very broad minima (see Fig. 3). The double minima in the

curve calculated at the MP2/6-311++G(d,p) level of theory are asymmetric due to the coupling with the 2-methyl rotor, as indicated in the lower panel of Fig. 3 where the oscillation of the 2-methyl rotor upon internal rotation of the 5-methyl rotor is visualized.

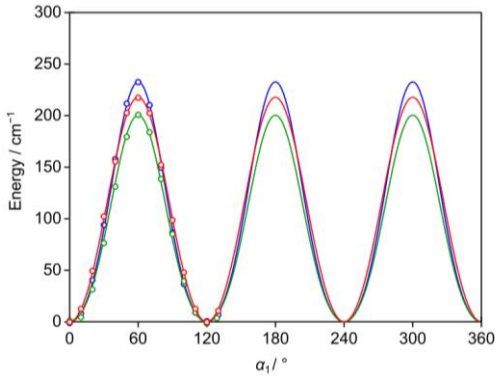

FIG. 2. The potential energy curves of 25DMFB computed at the B3LYP-D3BJ/6-311++G(d,p) (red curve), MP2/6-311++G(d,p) (blue curve), and MP2/6-31G(d,p) (green curve) levels of theory by adjusting the dihedral angle α_1 = ∠(C_3,C_2,C_7,H_{12}) in 10° increments, representing the rotation of the 2-methyl group about the C_2–C_7 bond (for atom numbering, see Fig. 1). The predicted torsional barriers are 217.8 cm^{-1}, 232.8 cm^{-1}, and 200.5 cm^{-1}, respectively.

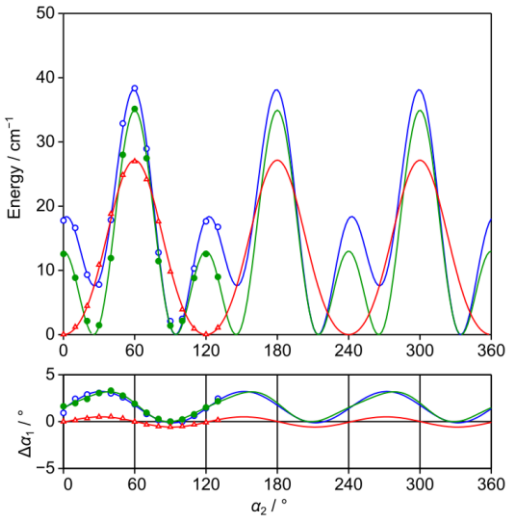

FIG. 3. Upper trace: The potential energy curves of 25DMFB computed at the B3LYP-D3BJ/6-311++G(d,p) (red curve), MP2/6-311++G(d,p) (blue curve), and MP2/6-31G(d,p) (green curve) levels of theory by adjusting the dihedral angle α_2 = ∠(C_4,C_5,C_8,H_{15}) in 10° increments, corresponding to the rotation of the 5-methyl group about the C_5–C_8 bond (for atom numbering, see Fig. 1). The V_3/V_6 ratios of 27.2/3.2 cm^{-1}, 20.1/23.2 cm^{-1}, and 21.9/22.6 cm^{-1}, respectively, are needed to

reproduce the obtained energy points. Lower trace: Oscillation of the 2-methyl group upon the rotation of the 5-methyl group. The values are given relative to the α_1 angle of the geometry at the minimum of each curve (0.00643° for B3LYP-D3BJ, 0.23961° for MP2/6-311++G(d,p), and 1.63057° for MP2/6-31G(d,p)).

Commenté [LN1]: I find this very strange at the MP2/6-31G(d,p) has a significantly larger angle at minimum than MP2/6-311++G(d,p). I would expect the same angle for both.

Commenté [SK2R1]: I checked it again, this is what I found

The asymmetry of the potential curve calculated at the MP2/6-311++G(d,p) level suggested a strong coupling between the two methyl rotors. When a methyl group rotates, it induces oscillation of the other methyl group (see the lower panel of Fig. 3), therefore influencing the potential energy of the entire molecule. To understand this coupling in 25DMFB, we calculated two-dimensional potential energy surfaces (2D-PES) by varying both dihedral angles α_1 and α_2 in a grid of 10°. All other geometry parameters were optimized at the three levels of theory mentioned above. Using a 2D-Fourier expansion taking into account the C_3 symmetry of the methyl groups, the calculated energies were parameterized with Fourier coefficients shown in Table S-IV in the Supplementary Materials. The 2D-PES are drawn using these coefficients, and those obtained from the MP2/6-311++G(d,p) and B3LYP-D3BJ/6-311++G(d,p) levels are given in Fig. 4. The 2D-PES calculated at the MP2/6-3G(d,p) level is very similar to that obtained at the MP2/6-311++G(d,p) level and is given in Fig. S-II of the Supplementary Materials. The minimum regions of the B3LYP-D3BJ 2D-PES have stretched oblate shapes, indicating that the two methyl internal rotations strongly couple with each other, as they would be circles otherwise. At both MP2 levels, double minimum regions are observed, and large values are found for the V_6 term of the 5-methyl group, the $\cos(3\alpha_1)\cos(3\alpha_2)$, and $\sin(3\alpha_1)\sin(3\alpha_2)$ terms (see Table S-IV). This also indicates that the two methyl torsions are coupled.

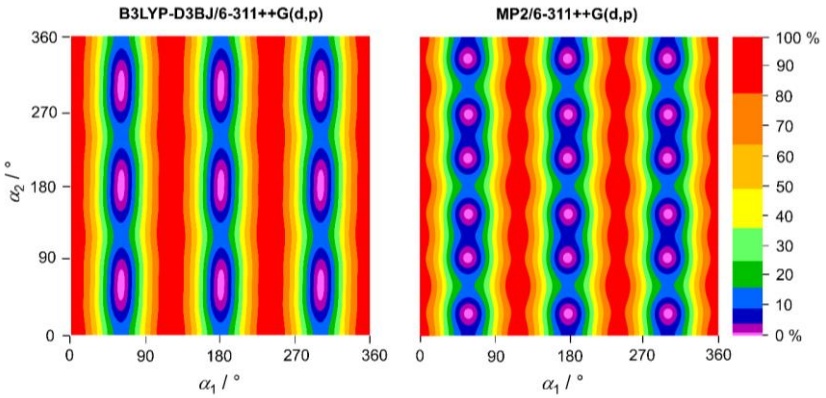

FIG. 4. 2D-PES of 25DMFB calculated at the B3LYP-D3BJ/6-311++G(d,p) and MP2/6-311++G(d,p) levels of theory in dependence of the dihedral angles $\alpha_1 = \angle(C_3,C_2,C_7,H_{12})$ and $\alpha_2 = \angle(C_4,C_5,C_8,H_{15})$. The two dihedral angles were varied in 10° steps, and all other geometry parameters were optimized. The numbers in the color code indicate the energy (in percent) relative

to the energetic maximum (100%) and minimum (0%) with E_{max} (B3LYP-D3BJ) = – 410.265285 Hartree (100%), E_{max} (MP2) = –409.062879 Hartree (100%), E_{min} (B3LYP-D3BJ) = –410.266304 Hartree (0%), and E_{min} (MP2) = –409.064260 Hartree (0%). The respective relative energies $E_{max} - E_{min}$ are 223.6 cm^{-1} and 303.1 cm^{-1}.

III. MICROWAVE SPECTROSCOPY

A. Experiments

The spectrum of 25DMFB was recorded with a pulsed molecular jet Fourier transform microwave spectrometer operating in the frequency range from 2 to 26.5 GHz with a coaxial arrangement between the molecular jet and the resonator (COBRA).[54] The substance with a purity of 98% was purchased from TCI Europe, Zwijndtrecht, Belgium. Several drops of 25DMFB were put on a piece of a pipe cleaner that was subsequently placed inside a steel tube upstream of the nozzle. 25DMFB was transported into the vacuum chamber using helium as carrier gas at an absolute pressure of 2 bar. At the beginning, we recorded a scan from 10.7 to 12.9 GHz by taking automatically overlapping spectra with 50 co-decays per each at a step width of 250 kHz which is the resolution of the survey spectrum. A portion of the scan is visualized in Fig. 5. After the spectrum had been assigned, high-resolution measurements with a measurement accuracy of 4 kHz were carried out, where the lines appeared as doublets due to the Doppler effect arising from the COBRA arrangement. Typical high-resolution spectra of the *a*-type $6_{16} \leftarrow 5_{15}$ transition with its five torsional species (00), (01), (10), (11), and (12) are shown in Fig. 6.

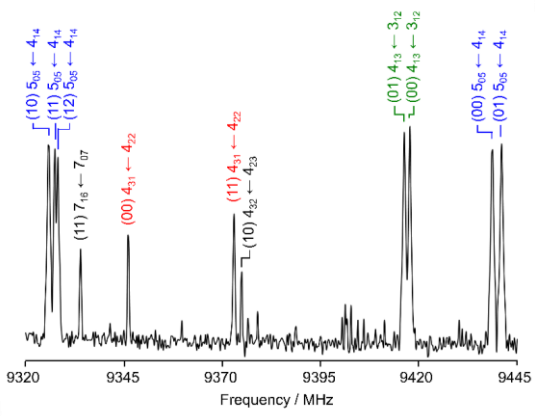

FIG. 5. A portion of the survey scan of 25DMFB in the frequency range from 9320 to 9445 MHz recorded by overlapping spectra with 50 co-added decays per each spectrum at a resolution of 0.25 MHz. The arbitrary intensity is given in logarithmic

scale. Assigned lines are labelled by their rotational quantum numbers $J''_{K''_a K''_c} \leftarrow J'_{K'_a K'_c}$ and the torsional species ($\sigma_1\sigma_2$). Torsional species belonging to the same rotational transition are color-coded.

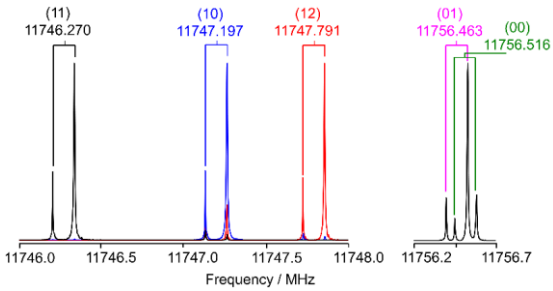

FIG. 6. Typical spectra at high-resolution (4 kHz measurement accuracy) of the *a*-type $6_{16} \leftarrow 5_{15}$ transition with splitting into five torsional components (00), (01), (10), (11), and (12). The Doppler doublets are marked by brackets. For the left hand side spectrum, three high-resolution measurements (shown in different colors) are combined. The intensities are normalized and do not represent the spin statistical weight.

B. Spectral assignment and fits

To start the assignment of the microwave spectrum of 25DMFB, we first used a rigid-rotor Hamiltonian model with no internal rotation effects. According to the predicted dipole moment components given in Table I, *a*- and *b*-type transitions should be equally intense, and *c*-type transitions do not exist. Using the rotational constants calculated at the B3LYP-D3BJ/6-311++G(d,p) level of theory, we predicted a rigid-rotor spectrum with the *XIAM* program[4] which was compared to the recorded scan. The rigid-rotor assignment was straightforward with some *a*-type *R*-branch transitions with K_a = 0, 1 assigned first, then also some *b*-type ones.

For some *a*-type transitions assigned in the rigid-rotor fit, doublets were observed in the scan and triplets with the same intensity were found in close proximity. Since the internal rotation of the 2-methyl group should be hindered by an intermediate barrier of about 220 cm^{-1},[32,33,55] and that of the 5-methyl group by a very low barrier, the doublets showed most probably the (00)-(01) splittings, and the triplets the (10)-(11)-(12) splittings. We then analyzed the high-resolution measurements of those transitions to assign the torsional species. Using the V_3 value of 218 cm^{-1} (close to the value of 220 cm^{-1} from our experience[55]) for the 2-methyl group and the value of 27 cm^{-1} for the 5-methyl group (no experience) calculated at the B3LYP-D3BJ/6-311++G(d,p) level of theory (see Table I), we predicted the splittings of the five torsional species with *XIAM*. From the predicted frequency order of the torsional species in the splittings, we could confidentially assign the (00) and (01) species, as well as started the

assignment of the (10), (11), and (12) species. To assign the fine splittings of *b*-type transitions, we used combination difference loops (Ritz cycles)[56] which allowed us to check the correctness of the (10), (11), and (12) species assignment. A simplified description of a Ritz cycle is given in Fig. S-III in the Supplementary Materials. After many trial and error with careful checking, a sufficient number of (10), (11), and (12) lines could be confidentially assigned with loop sums lower than 10 kHz. Separate fits were then carried out for these three species with the *SFLAMS* program[57] using the following Hamiltonian:

$$\mathbf{H} = \mathbf{H_{rot}} + \mathbf{H_{cd}} + \mathbf{H_{op}}. \quad (2)$$

For the (00) species, only the semi-rigid rotor part of the Hamiltonian ($\boldsymbol{H_{rot} + H_{cd}}$) including the three rotational constants and five quartic centrifugal distortion constants was needed. For all torsional excited species, we had to float the odd power parameter q (also called D_a in the literature) and its higher order terms q_J, q_K, and q_{KK}, as well as the r parameter (also called D_b) and its higher order terms r_J and r_K included in the $\boldsymbol{H_{op}}$ part:

$$\mathbf{H_{op}} = \left(q + q_J\mathbf{P}^2 + q_K\mathbf{P_z^2} + q_{KK}\mathbf{P_z^4}\right)\mathbf{P_z} + (r + r_J\mathbf{P}^2)\mathbf{P_x} + \frac{1}{2}r_K\{\mathbf{P_z^2}, \mathbf{P_x}\}. \quad (3)$$

where {A, B} is the anti-commutator AB + BA. Predictions from the separate fits allowed us to find more lines, which were also checked by Ritz cycles[56] as illustrated in Fig. 7. The separate fits are shown in Table II. The rms deviations for all torsional species fits are close to the measurement accuracy of about 4 kHz, which is also the average of all loop sums. Note that more (10), (11), and (12) species lines have been measured to ensure the correct assignments and the reliability of the *SFLAMS* predictions. Also note that all *SFLAMS* fits are effective and the fitted parameters have lost their physical meaning, especially the centrifugal distortion constants which no longer represent the centrifugal distortion effects. The lower the barriers, the more effective these parameters become since they have to partly compensate the splittings arising from the methyl internal rotation. It is recognizable that the centrifugal distortion constant values of the (00) and (01) species as well as those of the (10), (11), and (12) species are more similar among each group, because the species are associated with the 2- and the 5-methyl rotors, respectively. The centrifugal distortion constants are also strongly correlated with the odd power parameters. We can see that the *K*-dependent constants, i.e. Δ_{JK}, Δ_K, and δ_K, differ the most between the two species groups as the q_K and r_K values of the (10), (11), and (12) species are much larger than the values of the (00), which is zero, and (01) species.

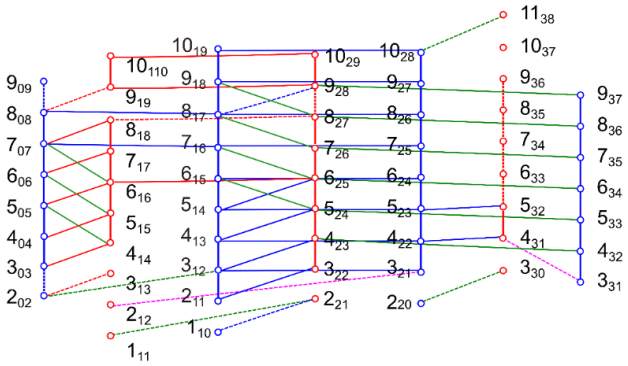

FIG. 7. A schematic illustration depicting nearly all rotational transitions of the (10), (11), and (12) torsional species of 25DMFB. The solid lines connecting two circles signify transitions verified using combinations difference loops, which sum to the measurement accuracy of 4 kHz. Several transitions with low intensity could not be measured, resulting in open loops. Transitions shown as dashed lines are not loop-checked.

TABLE II. Molecular parameters of the (00), (01), (10), (11), and (12) separate fits obtained with the program *SFLAMS*.

Par.[a]	Unit	(00)	(01)	(10)	(11)	(12)
A	MHz	3074.56929(28)	3072.00917(24)	3029.52322(29)	3027.25661(31)	3026.85307(38)
B	MHz	1285.58883(14)	1285.55998(13)	1285.251761(66)	1285.224129(67)	1285.221647(74)
C	MHz	912.19851(12)	912.20228(12)	912.244104(58)	912.248229(57)	912.247260(68)
Δ_J	kHz	0.0225(15)	0.0249(15)	0.01611(36)	0.01605(36)	0.01705(57)
Δ_{JK}	kHz	0.1171(49)	0.0570(73)	0.6470(24)	0.6363(24)	0.6258(50)
Δ_K	kHz	1.597(23)	1.413(23)	21.959(30)	21.431(30)	21.343(41)
δ_J	kHz	0.00805(43)	0.00804(40)	0.00847(24)	0.00819(24)	0.00812(35)
δ_K	kHz	0.00180(21)	0.00097(20)	0.005412(83)	0.005352(84)	0.00462(13)
q	MHz		77.03927(45)	4073.89067(51)	3991.70313(53)	4138.42528(79)
r	MHz		7.115(39)	399.76812(80)	392.37305(75)	406.6091(11)
q_J	kHz		–0.316(20)	–13.3137(84)	–12.8679(86)	–13.475(15)
q_K	kHz		–18.901(56)	–1142.239(69)	–1115.237(71)	–1155.84(17)
q_{KK}	kHz			–0.3088(39)	–0.2881(41)	–0.246(12)
r_J	kHz			–0.8367(97)	–0.7971(96)	–0.846(19)
r_K	kHz			–289.44(27)	–281.83(26)	–294.26(32)
N[b]		55	61	117	120	104
rms[c]	kHz	1.9	2.0	4.3	3.3	2.8

[a] All parameters refer to the principal axis system. Watson's A reduction in I^r representation was used. [b] Number of lines. [c] Root-mean-square deviation of the fit.

Finally, 457 lines fitted separately with *SFLAMS* were input in a global fit using a modified version of the *XIAM* program[57,58] that includes two higher order parameters more than the original version of *XIAM*.[4] *XIAM* uses a combined-axis method where the rho-axis system was used to set up the Hamiltonian $\mathbf{H}_{i,\mathrm{RAM}}$ for each methyl internal rotation before being rotated into the principal axis system with the rotation matrix:

$$\boldsymbol{D}(\beta,\gamma)=\begin{pmatrix} cos\beta & 0 & -sin\beta \\ 0 & 1 & 0 \\ sin\beta & 0 & cos\beta \end{pmatrix}\begin{pmatrix} cos\gamma & sin\gamma & 0 \\ -sin\gamma & cos\gamma & 0 \\ 0 & 0 & 1 \end{pmatrix}. \quad (4)$$

In equation (4), the Euler angles β and γ are defined as $cos\beta = {}^{\rho_z}/_{\rho}$ and $cos\gamma = \rho_x\sqrt{\rho_x^2+\rho_y^2}$, where ρ is a vector parallel to the rho-axis describing the coupling term and ρ_x , ρ_y, ρ_z are the three components in the principal axis system. The Hamiltonian in the principal axis system can be written as:

$$\mathbf{H} = \mathbf{H_{rot}} + \mathbf{H_{cd}} + \mathbf{D^{-1}H_{i,RAM}D}. \quad (5)$$

Fitted internal rotation parameters are the V_3 potentials, angles $\angle(i_1,a)$ and $\angle(i_2,a)$ between the *a*-principal axis and the internal rotor axes, the top-top coupling term V_{cc} multiplying $\cos(3\alpha_1)\cos(3\alpha_2)$, and the internal rotation distortion terms $D_{\pi^2 J}$, $D_{\pi^2 K}$, D_{π^2-}, D_{c3K} for the 5-methyl group. They multiply $2(p_{\alpha_2}-\vec{\rho}^{\dagger}\vec{P})^2P^2$, $\{(p_{\alpha_2}-\vec{\rho}^{\dagger}\vec{P})^2, P_a^2\}$, $\{(p_{\alpha_2}-\vec{\rho}^{\dagger}\vec{P})^2, (P_b^2-P_c^2)\}$,[59] and $\cos(3\alpha_2)P_a^2$,[57] respectively. p_{α_2} is the momentum operator of the 5-methyl group, and $\boldsymbol{P}$ the angular momentum operator in the principal axis system with the three components $\boldsymbol{P_a}$, $\boldsymbol{P_b}$, and $\boldsymbol{P_c}$. The rotational constants of both methyl rotors F_0 are correlated with V_3 and were fixed to 158 GHz, a value often found for methyl groups. The *XIAM* fit given in Table III achieves a standard deviation of 384.3 kHz, almost a hundred times the measurement accuracy. To improve the global fitting, we used the *BELGI-C_s-2Tops* program[7] to fit the same data set and achieved an rms deviation of 4.7 kHz, very close to the measurement accuracy of 4 kHz. In this fit, the constants f_1 and f_2 related to the methyl rotational constants as well as the kinetic coupling term f_{12} were kept fixed. Note that $f_1 = F_1$, $f_2 = F_2$, and $f_{12} = F_{12}$.[31] We floated 29 parameters including the three rotational constants, the centrifugal distortion constants (except δ_K which was not determined and was fixed to zero), the two V_3 potentials and their *J* and *K* dependence terms, Q_1, Q_2, R_1, and R_2 related to the values of ρ by the relations:

$$q_1 = -2f_1\rho_{1a}\,;\; q_2 = -2f_2\rho_{2a} \quad (6a)$$

$$r_1 = -2f_1\rho_{1b}\,;\; r_2 = -2f_2\rho_{2b} \quad (6b)$$

and their *J* and *K* dependence terms. We also had to float B_1 and B_2 which multiply the operators $p_1^2P_z^2$ and $p_2^2P_z^2$, respectively. Two interaction terms in the potential, V_{12c} and V_{12s}, were also fitted. The parameters

Commenté [LN3]: I count only 24 in Table IV.

Commenté [LN4]: I only see the K dependence terms fitted in Table IV

Commenté [LN5]: In Table IV, only p2^2*Pz^2 is fitted and noted as f2K and not B2.

obtained from the *BELGI-C_s-2Tops* fit in the "quasi-PAM" system are given in Table IV. Molecular parameters that can be converted into the principal axis system are shown in Table III for a comparison with the *XIAM* values.

TABLE III. Molecular parameters of 25DMFB in the principal axis system obtained using the *XIAM$_{mod}$* and *BELGI-C_s-2Tops* programs.

Par.[a]	Unit	Fit *XIAM*	Fit *BELGI*	Calc.[b]
A	MHz	3023.640(20)	3032.84(31)	3022.5
B	MHz	1285.1196(52)	1285.3083(50)	1285.0
C	MHz	912.1934(45)	912.5488(36)	911.8
Δ_{JK}	kHz	0.80(20)		0.13462
Δ_K	kHz	–5.32(76)		0.35008
$V_{3,1}$	cm^{-1}	226.274(31)	237.76(11)	217.8
$V_{3,2}$	cm^{-1}	16.386(67)	28.836(39)	26.3
V_{cc}	cm^{-1}	–6.992(53)	–6.245(49)	–5.38
V_{ss}	cm^{-1}		25.80(32)	
ρ_1	unitless	0.01875[c]	0.018760(18)	
ρ_2	unitless	0.01874[c]	0.018502(18)	
F_1	GHz	161.0491[c]	161.0491[d]	
F_2	GHz	161.0527[c]	161.0527[d]	
$D_{\pi^2 J,2}$	kHz	43.8(2.2)		
$D_{\pi^2 K,2}$	MHz	2.16(16)		
$D_{\pi^2 -,2}$	kHz	25.7(1.5)		
$D_{c3K,2}$	GHz	0.0124(16)		
$\angle(i_1,a)$	°	12.729(70)	12.80(33)	11.2
$\angle(i_1,b)$	°	77.270(70)	77.204(17)	78.8
$\angle(i_1,c)$	°	90.0[e]	90.0[e]	90.0
$\angle(i_2,a)$	°	167.0073(12)	166.96(33)	166.2
$\angle(i_2,b)$	°	102.9927(12)	103.037(17)	103.8
$\angle(i_2,c)$	°	90.0[e]	90.0[e]	90.0
N[f]		457	457	
rms[g]	kHz	384.3	4.7	

[a] All molecular parameters refer to the principal axis system. Watson's A reduction and I^r representation were used. [b] Calculated at the B3LYP-D3BJ/6-311++G(d,p) level of theory. The rotational constants refer to the equilibrium structure. [c] Derived parameters in *XIAM$_{mod}$*. [d] Fixed to the value from the *XIAM$_{mod}$* fit. [e] Fixed due to symmetry. [f] Number of lines. [g] Root-mean-square deviation of the fit.

Commenté [LN6]: Is Dc3K,2 this big? Please check. If it is correct, change unit to MHz.

Commenté [SK7R6]: I checked it, it's the right value.

TABLE IV. Molecular parameters of 25DMFB in the "quasi-PAM" axis system obtained using the *BELGI-C_s-2Tops* program.

Operator[a]	Par.[b]	Unit	value
$\mathbf{P_z^2}$	A	MHz	3144.67(29)
$\mathbf{P_x^2}$	B	MHz	1286.3004(49)
$\mathbf{P_y^2}$	C	MHz	912.5488(36)
$-\mathbf{P^4}$	Δ_J	kHz	0.02395(55)
$-\mathbf{P^2P_z^2}$	Δ_{JK}	kHz	–0.1016(90)
$-\mathbf{P_z^2}$	Δ_K	kHz	0.660(17)
$-2\mathbf{P^2}(\mathbf{P_x^2}-\mathbf{P_y^2})$	δ_J	kHz	0.00774(29)
$(1/2)(1-\cos 3\alpha_1)$	$V_{3,1}$	cm^{-1}	237.76(11)
$\mathbf{P_zp_1}$	q_1	GHz	–6.0721(57)
$\mathbf{P_xp_1}$	r_1	GHz	0.54877(53)
$(1/2)\{\mathbf{P_z^2},\mathbf{P_x}\}\mathbf{p_1}$	r_{1K}	MHz	0.1479(77)
$\mathbf{p_1^2}$	f_1	GHz	161.0527[c]
$(1/2)(1-\cos 3\alpha_1)\mathbf{P^2}$	$V_{3,1J}$	MHz	0.301(14)
$(1/2)(1-\cos 3\alpha_1)\mathbf{P_z^2}$	$V_{3,1K}$	MHz	–27.86(75)
$(1/2)(1-\cos 3\alpha_1)\{\mathbf{P_x^2}-\mathbf{P_y^2}\}$	$V_{3,1BC}$	MHz	1.112(11)
$(1/2)(1-\cos 3\alpha_2)$	$V_{3,2}$	cm^{-1}	28.836(39)
$\mathbf{P_zp_2}$	q_2	GHz	5.9887(27)
$\mathbf{P_z^3p_2}$	q_{2K}	MHz	–0.0250(11)
$\mathbf{P_xp_2}$	r_2	GHz	–0.55225(23)
$\mathbf{p_2^2}$	f_2	GHz	161.0491[c]
$\mathbf{p_2^2P_z^2}$	f_{2K}	MHz	–1.390(64)
$(1/2)(1-\cos 3\alpha_2)\mathbf{P^2}$	$V_{3,2J}$	MHz	–0.4455(23)
$(1/2)(1-\cos 3\alpha_2)\{\mathbf{P_z},\mathbf{P_x}\}$	$V_{3,2AB}$	MHz	0.789(38)
$(1/2)(1-\cos 3\alpha_2)\{\mathbf{P_x^2}-\mathbf{P_y^2}\}$	$V_{3,2BC}$	MHz	–0.2211(26)
$(1-\cos 3\alpha_1)(1-\cos 3\alpha_2)$	V_{12c}	cm^{-1}	–6.245(49)
$\sin\alpha_1\sin\alpha_2$	V_{12s}	cm^{-1}	25.80(32)
	N[d]		457
	rms[e]	kHz	4.7

[a] Operator which the parameters multiply in the program. [b] All parameters refer to the quasi-PAM system. [c] Fixed to the value from the *XIAM$_{mod}$* fit. [d] Number of lines. [e] Root-mean-square deviation of the fit.

IV. RESULTS AND DISCUSSION

The microwave spectra of 25DMFB were analyzed and 457 rotational lines were fitted using the programs *XIAM$_{mod}$* and *BELGI-C_s-2Tops*. The assignments were checked by combination difference loops and fitting the torsional species separately. The *XIAM$_{mod}$* fit achieved an rms deviation of 384.3 kHz. The *BELGI-C_s-2Tops* code, with additional higher order effective parameters, reduced the deviation to 4.7 kHz, which is satisfactorily close to the measurement accuracy of 4 kHz.

Benchmark calculation results in Table S-II of the Supplementary Materials (see section II.B.) show that the equilibrium rotational constants B_e obtained at all levels of theory are generally in good agreement with the experimental constants B_0 obtained by the *XIAM$_{mod}$* program with deviations smaller than 1.7 % for *A*, 1.4 % for *B*, and 1.5% for *C*. The B_e constants presented in Table I are in very good agreement with the B_0 ones with

deviations lower than 0.1% obtained at the B3LYP-D3BJ/6-311++G(d,p) and MP2/6-31G(d,p) levels, and lower than 0.5% at the MP2/6-311 ++G(d,p) level. For the 2,3-, 2,6-, and 3,4-isomers of DMFB, rotational constants calculated at the B3LYP-D3BJ/6-311++G(d,p) and MP2/6-31G(d,p) levels were recommended to guide the assignment of the microwave spectra.[32-34] In the present case of 25DMFB, the values of the three rotational constants obtained at the B3LYP-D3BJ/6-311++G(d,p) level are in almost exact agreement with the experimental ones, with percentage errors that do not exceed 0.04%, and the MP2/6-31G(d,p) level also performs very well. Therefore, we continue recommending them for assignment guidance of related molecules. The MP2/6-311++G(d,p) level that we often used for geometry optimizations of aromatic ring containing molecules[60-62] also yielded good results for 25DMFB. We note that from theoretical perspective, predicted B_0 values obtained from anharmonic frequency calculations should be more accurate and closer to the experimental B_0 values. However, the errors of certain levels might compensate with the missing $B_e - B_0$ in a way that the calculated B_e rotational constants accidentally match the experimental B_0 constants, making these levels useful for assigning microwave spectra at an efficient cost.

The torsional barriers for the 2- and 5-methyl groups are determined with the *XIAM*$_{mod}$ program to be 226.274(31) cm^{-1} and 16.386(67) cm^{-1}, respectively. The respective values obtained with *BELGI-*C_s*-2Tops* are 237.76(11) cm^{-1} and 28.836(39) cm^{-1}. Though in the same order of magnitude, the *BELGI* values are about 12 cm^{-1} higher for both rotors. This interesting observation supports the argument that the differences in torsional barrier values are due to different methods used by each program and also due to the correlations between the many effective parameters floated in the *BELGI* program to treat the very low torsional barrier of the 5-methyl group. Because of the large differences, the *XIAM* values are taken as reference for comparison with the theoretical ones, since *XIAM* parameters are physically more meaningful with lower correlations.

For the 2-methyl group, the barrier heights predicted at the B3LYP-D3BJ/6-311++G(d,p), MP2/6-311++G(d,p), and MP2/6-31G(d,p) levels are 217.8 cm^{-1}, 232.78 cm^{-1}, and 200.48 cm^{-1}, respectively, which are all relatively close to the experimental value of 226 cm^{-1}. A comparison between the calculated and the experimental values is difficult for the 5-methyl group due to the significant V_6 contribution which even dominates the V_3 term in calculations at the MP2/6-311++G(d,p) and MP2/6-31G(d,p) levels of theory (see section II.C). Lacking transitions of vibrational excited state in the data set, we were unable to fit the V_6 term to confirm this experimentally.

As shown in Fig. 8, the torsional barrier of 226.3 cm^{-1} for the 2-methyl group of 25DMFB (**1**) is very close to the values found for 24DMFB (**2**, 227.0 cm^{-1}),[63] 26DMFB (**3**, 236.8 cm^{-1}),[33] and 23DMFB (**4**, 215.6 cm^{-1}).[32]

This value is also close to that of *o*-fluorotoluene (**5**),[64] difluorotoluene,[65-67] trifluorotoluene,[68] or even mixed halotoluene,[69] confirming our previous finding that the barrier to internal rotation of a methyl group neighboring a fluorine atom is always around 220 cm^{-1}.

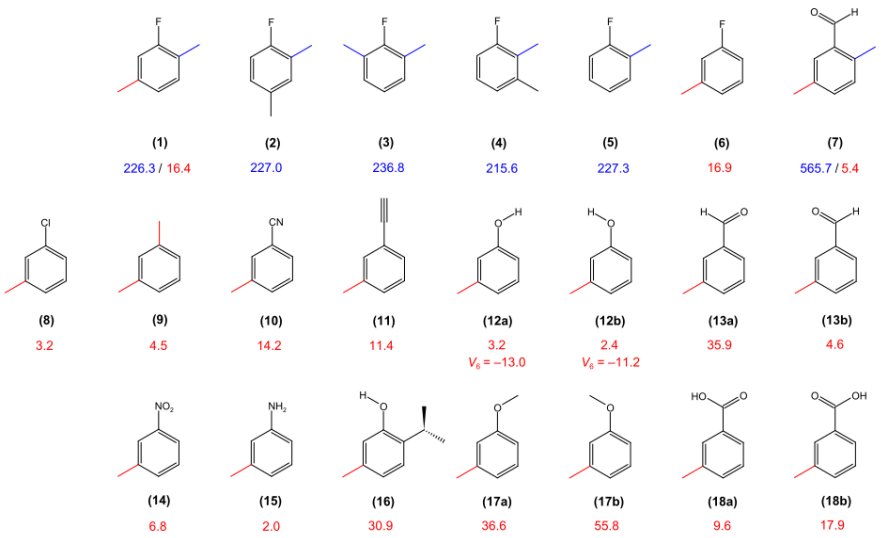

FIG. 8. Comparison of the barriers to methyl internal rotation (given in cm^{-1} and color-coded to the methyl group) in dimethylfluorobenzene isomers and *meta*-substituted toluene derivatives. (**1**) 2,5-dimethylfluorobenzene (this work), (**2**) 2,4-dimethylfluorobenzene,[63] (**3**) 2,6-dimethylfluorobenzene,[33] (**4**) 2,3-dimethylfluorobenzene,[32] (**5**) *o*-fluorotoluene,[64] (**6**) *m*-fluorotoluene,[70] (**7**) *syn*-2,5-dimethylbenzaldehyde,[71] (**8**) *m*-chlorotoluene,[72] (**9**) *m*-xylene,[73] (**10**) *m*-tolunitril,[74] (**11**) *m*-methylphenylacetylene,[23] (**12a**) *anti*-*m*-cresol,[75] (**12b**) *syn*-*m*-cresol,[75] (**13a**) *anti*-*m*-methylbenzaldehyde,[76] (**13b**) *syn*-*m*-methylbenzaldehyde,[76] (**14**) *m*-nitrotoluene,[77] (**15**) *m*-toluidine,[78] (**16**) *syn*-thymol,[19] (**17a**) *anti*-*m*-methylanisole,[10] (**17b**) *syn*-*m*-methylanisole,[10] (**18a**) *anti*-*m*-toluic acid,[79] (**18b**) *syn*-*m*- toluic acid.[79]

The torsional barrier of 16.4 cm^{-1} found for the *m*-methyl group of 25DMFB (**1**) is very low. For the *m*-methyl group in other toluene derivatives reported in the literature where steric-hindrance is absent,[10,19,23,70-79] we found the highest value of 55.8 cm^{-1} for *syn*-*m*-methylanisole (**17b**)[10] and the lowest one of 2.0 cm^{-1} for *m*-toluidine (**15**).[78] Despite the same position of the methyl group in these molecules on the toluene ring and the same steric-free environment, the barrier values ranging from 2.0 cm^{-1} to 55.8 cm^{-1} are quite different, probably because the electronic environment surrounding the methyl group is also influenced by the other substituent(s) attached to the phenyl group through the π-conjugated system. Fitting approaches also play an important role, i.e. whether the V_6 term can be fitted or not. Coupling between the internal rotations also affects the observed torsional barriers, as

can be seen from the different values obtained with the *XIAM* and *BELGI* fits and the significant V_{cc} terms in *XIAM*. In conclusion, the evident influence of the electronic environment on the methyl internal rotation barrier within π-conjugated systems highlights the potential of this physical parameter as a sensitive indicator of molecular electronic distribution. However, the precise mechanisms driving this phenomenon remain elusive. Electronic effects appear considerably complex compared to steric hindrance and are challenging to precisely characterize. While our present study on 25DMFB has contributed a significant data point, furthers experimental investigation and in-depth quantum chemical analyses are required to understand them.

V. Conclusion

Using a molecular jet Fourier transform microwave spectrometer, microwave spectra of 25DMFB were captured within the frequency range of 2.0 to 26.5 GHz. Torsional splitting due to internal rotation of the two inequivalent methyl groups at the *ortho* and *meta* positions was observed. The *XIAM*$_{mod}$ and *BELG-C*$_s$*-2Tops* programs were utilized to analyze and fit the complex splitting patterns, yielding rms deviations of 384.3 kHz and 4.7 kHz, respectively. Assignments and predictions of torsional lines were checked by combination difference loops and by fitting the five torsional components separately. The experimental V_3 potential values were determined to be 226.274(31) cm^{-1} and 16.386(67) cm^{-1} for the 2- and 5-methyl groups, respectively. The 2D-PES demonstrated significant coupling between the methyl groups, evidenced by a substantial V_{cc} contribution present in the fits. Comparison of the potential barriers found for the 2-methyl group with those of the other *ortho*-substituted toluene derivatives confirms that the internal rotation barrier for the methyl groups adjacent to the fluorine atom is consistently around 220 cm^{-1}. The V_3 barrier of 16.386(67) cm^{-1} obtained for the *m*-methyl group is very low, similar to the value observed so far for steric-free *m*-methyl groups in other toluene derivatives reported in the literature.

SUPPLEMENTARY MATERIAL

See the supplementary materials for the nuclear coordinates for the optimized structures, equilibrium rotational constants predicted at different levels of theory, Fourier coefficients of the potential curves and the 2D-PES, potential energy surface depending on the dihedral angles α_1 and α_2 calculated at the at the MP2/6-31G(d,p) level of theory, and frequency list.

ACKNOWLEDGMENTS

H.S. thanks the Chinese Scholarship Councils (CSC) from the Chinese government for a PhD scholarship. This work was supported by the Agence Nationale de la Recherche ANR (project ID ANR-18-CE29-0011) and by the European Union (ERC, 101040480-LACRIDO). Views and opinions expressed are however those of the authors only and do not necessarily reflect those of the European Union. Neither the European Union nor the granting authority can be held responsible for them.

DATA AVAILABILITY

The data that support the findings of this study are available within the article and its supplementary material. The programs *SFLAMS*, *aixPAM*, and *ntop* are available with H.V.L.N. and can be shared on request.

REFERENCES

[1] H. V. L. Nguyen and I. Kleiner, Phys. Sci. Rev. **7**, 679 (2020).
[2] H. V. L. Nguyen, I. Gulaczyk, M. Kręglewski, and I. Kleiner, Coord. Chem. Rev. **436**, 213797 (2021).
[3] A. C. Legon, Chem. Rev. **80**, 231 (1980).
[4] H. Hartwig and H. Dreizler, Z. Naturforsch. **51a**, 923 (1996).
[5] J. T. Hougen, I. Kleiner, and M. Godefroid, J. Mol. Spectrosc. **163**, 559 (1994).
[6] I. Kleiner and J. T. Hougen, J. Chem. Phys. **119**, 5505 (2003).
[7] M. Tudorie, I. Kleiner, J. T. Hougen, S. Melandri, L. W. Sutikdja, and W. Stahl, J. Mol. Spectrosc. **269**, 211 (2011).
[8] V. V. Ilyushin, Z. Kisiel, L. Pszczólkowski, H. Mäder, and J. T. Hougen, J. Mol. Spectrosc. **259**, 26 (2010).
[9] V. V. Ilyushin and J. T. Hougen, J. Mol. Spectrosc. **289**, 41 (2013).
[10] L. Ferres, W. Stahl, and H. V. L. Nguyen, J. Chem. Phys. **148**, 124304 (2018).
[11] L. Ferres, W. Stahl, and H. V. L. Nguyen, J. Chem. Phys. **151**, 104310 (2019).
[12] P. Groner, J. Chem. Phys. **107**, 4483 (1997).
[13] Z. Kisiel, http://info.ifpan.edu.pl/~kisiel/prospe.htm
[14] S. Herbers, O. Zingsheim, H. V. L. Nguyen, L. Bonah, B. Heyne, N. Wehres, and S. Schlemmer, J. Chem. Phys., **155**, 224302 (2021).
[15] E. J. Cocinero, F. J. Basterretxea, P. Écija, A. Lesarri, J. A. Fernández, and F. Castaño, Phys. Chem. Chem. Phys. **13**, 13310 (2011).
[16] R. Kannengießer, S. Klahm, H. V. L. Nguyen, A. Lüchow, and W. Stahl, J. Chem. Phys. **141**, 204308 (2014).
[17] C. Calabrese, A. Maris, L. Evangelisti, A. Piras, V. Parravicini, and S. Melandri, Front. Chem. **6**, 1 (2018).
[18] K. J. Koziol, H. E. Hadki, A. Lüchow, N. Vogt, J. Demaison, and H. V. L. Nguyen, Spectrosc. J. **1**, 49 (2023).
[19] D. Schmitz, V. A. Shubert, B. M. Giuliano, and M. Schnell, J. Chem. Phys. **141**, 034304 (2014).
[20] C. Gregory, W. G. D. P. Silva, and J. van Wijngaarden, J. Mol. Spectrosc. **377**, 111444 (2021).
[21] K. Eibl, R. Kannengießer, W. Stahl, H. V. L. Nguyen, and I. Kleiner, Mol. Phys. **114**, 3483 (2016).

[22] K. Eibl, W. Stahl, I. Kleiner, and H. V. L. Nguyen, J. Chem. Phys. **149**, 144306 (2018).
[23] D. A. Obenchain, P. Pinacho, S. Zinn, and M. Schnell, J. Mol. Struct. **1213**, 128109 (2020).
[24] C. Dindić and H. V. L. Nguyen, Phys. Chem. Chem. Phys. **25**, 509 (2022).
[25] C. Dindić, M. Barth, and H. V. L. Nguyen, Spectrochim. Acta. A **280**, 121505 (2022).
[26] C. Dindić and H. V. L. Nguyen, ChemPhysChem **22**, 2420 (2021).
[27] M. Andresen, D. Schöngen, I. Kleiner, M. Schwell, W. Stahl, and H. V. L. Nguyen, ChemPhysChem **21**, 2206 (2020).
[28] H. V. L. Nguyen, H. Mouhib, W. Stahl, and I. Kleiner, Mol. Phys. **108**, 763 (2010).
[29] T. Nguyen, V. Van, C. Gutlé, W. Stahl, M. Schwell, I. Kleiner, and H. V. L. Nguyen, J. Chem. Phys. **152**, 134306 (2020).
[30] S. Khemissi, V. Van, M. Schwell, I. Kleiner, and H. V. L. Nguyen, J. Phys. Chem. A **127**, 5779 (2023).
[31] V. Van, T. Nguyen, W. Stahl, H. V. L. Nguyen, and I. Kleiner, J. Mol. Struct. **1207**, 127787 (2020).
[32] S. Khemissi, A. Pérez Salvador, and H. V. L. Nguyen, J. Phys. Chem. A **125**, 8542 (2021).
[33] S. Khemissi and H. V. L. Nguyen, ChemPhysChem **21**, 1682 (2020).
[34] J. Mélan, S. Khemissi, and H. V. L. Nguyen, Spectrochim. Acta. A **253**, 8 (2021).
[35] M. J. Frisch, G. W. Trucks, H. B. Schlegel, G. E. Scuseria, M. A. Robb, J. R. Cheeseman, G. Scalmani, V. Barone, G. A. Petersson, H. Nakatsuji, X. Li, M. Caricato, A. V. Marenich, J. Bloino, B. G. Janesko, R. Gomperts, B. Mennucci, H. P. Hratchian, J. V. Ortiz, A. F. Izmaylov, J. L. Sonnenberg, D. Williams-Young, F. Ding, F. Lipparini, F. Egidi, J. Goings, B. Peng, A. Petrone, T. Henderson, D. Ranasinghe, V. G. Zakrzewski, J. Gao, N. Rega, G. Zheng, W. Liang, M. Hada, M. Ehara, K. Toyota, R. Fukuda, J. Hasegawa, M. Ishida, T. Nakajima, Y. Honda, O. Kitao, H. Nakai, T. Vreven, K. Throssell, J. A. Montgomery Jr., J. E. Peralta, F. Ogliaro, M. J. Bearpark, J. J. Heyd, E. N. Brothers, K. N. Kudin, V. N. Staroverov, T. A. Keith, R. Kobayashi, J. Normand, K. Raghavachari, A. P. Rendell, J. C. Burant, S. S. Iyengar, J. Tomasi, M. Cossi, J. M. Millam, M. Klene, C. Adamo, R. Cammi, J. W. Ochterski, R. L. Martin, K. Morokuma, O. Farkas, J. B. Foresman, and D. J. Fox, Gaussian 16 (Gaussian, Inc., Wallingford, CT, 2016).
[36] A. D. Becke, J. Chem. Phys. **98**, 5648 (1984).
[37] C. Lee, W. Yang, and R. G. Parr, Phys. Rev. B. **37**, 785 (1988).
[38] S. Grimme, J. Antony, S. Ehrlich, and H. Krieg, J. Chem. Phys. **132**, 154104 (2010).
[39] S. Grimme, S. Ehrlich, and L. Goerigk, J. Comput. Chem. **32**, 1456 (2011).
[40] M. J. Frisch, J. A. Pople, and J. S. Binkley, J. Chem. Phys. **80**, 3265 (1984).
[41] C. Møller and M. S. Plesset, Phys. Rev. **46**, 618 (1934).
[42] I. Uriarte, A. Insausti, E. J. Cocinero, A. Jabri, I. Kleiner, H. Mouhib, and I. Alkorta, J. Phys. Chem. Lett. **9**, 5906 (2018).
[43] H. V. L. Nguyen and J.-U. Grabow, ChemPhysChem **21**, 1243 (2020).
[44] Z. Kisiel, O. Desyatnyk, L. Pszczółkowski, S. Charnley, and P. Ehrenfreund, J. Mol. Spectrosc. **217**, 115 (2003).
[45] H. V. L. Nguyen, J. Mol. Struct. **1208**, 127909 (2020).
[46] T. Yanai, D. P. Tew, and N. C. Handy, Chem. Phys. Lett. **393**, 51 (2004).
[47] Y. Zhao and D. G. Truhlar, Theor. Chem. Acc. **120**, 215 (2008).
[48] H. S. Yu, X. He, S. L. Li, and D. G. Truhlar, Chem. Sci. **7**, 5032 (2016).
[49] C. Adamo and V. Barone, J. Chem. Phys. **110**, 6158 (1999).

[50] J.-D. Chai and M. Head-Gordon, Phys. Chem. Chem. Phys. **10**, 6615 (2008).
[51] R. J. Bartlett and M. Musiał, Rev. Mod. Phys. **79**, 291 (2007).
[52] T. H. Dunning, J. Chem. Phys. **90**, 1007 (1989).
[53] L. Ferres, J. Cheung, W. Stahl, and H. V. L. Nguyen, J. Phys. Chem. A **123**, 3497 (2019).
[54] J.-U. Grabow, W. Stahl, and H. Dreizler, Rev. Sci. Instrum. **67**, 4072 (1996).
[55] H. V. L. Nguyen, W. Caminati, and J.-U. Grabow, Molecules **27**, 3948 (2022).
[56] Y. Zhao, H. V. L. Nguyen, W. Stahl, and J. T. Hougen, J. Mol. Spectrosc. **318**, 91 (2015).
[57] S. Herbers, S. M. Fritz, P. Mishra, H. V. L. Nguyen, and T. S. Zwier, J. Chem. Phys. **152**, 074301 (2020).
[58] S. Herbers and H. V. L. Nguyen, J. Mol. Spectrosc. **370**, 111289 (2020).
[59] N. Hansen, H. Mader, and T. Bruhn, Mol. Phys. **97**, 587 (1999).
[60] H. E. Hadki, K. J. Koziol, O. K. Kabbaj, N. Komiha, I. Kleiner, and H. V. L. Nguyen, Molecules **28**, 3419 (2023).
[61] S. Baweja, E. Antonelli, S. Hussain, A. Fernández-Ramos, I. Kleiner, H. V. L. Nguyen, and M. E. Sanz, Molecules **28**, 2153 (2023).
[62] C. Dindic, W. Stahl, and H. V. L. Nguyen, Phys. Chem. Chem. Phys. **22**, 19704 (2020).
[63] S. Khemissi, M. Schwell, I. Kleiner, and H. V. L. Nguyen, Phys. Chem. Chem. Phys. **26**, 402 (2024).
[64] S. Jacobsen, U. Andresen, and H. Mäder, Struct. Chem. **14**, 217 (2003).
[65] K. P. R. Nair, S. Herbers, J.-U. Grabow, and A. Lesarri, J. Mol. Spectrosc. **349**, 37 (2018).
[66] K. P. R. Nair, S. Herbers, D. A. Obenchain, J.-U. Grabow, and A. Lesarri, J. Mol. Spectrosc. **344**, 21 (2018).
[67] K. P. R. Nair, D. Wachsmuth, J.-U. Grabow, and A. Lesarri, J. Mol. Spectrosc. **337**, 46 (2017).
[68] K. P. R. Nair, S. Herbers, D. A. Obenchain, and J.-U. Grabow, Can. J. Phys. **98**, 543 (2020).
[69] K. P. R. Nair, S. Herbers, J.-U. Grabow, and H. V. L. Nguyen, J. Mol. Struct. **1246**, 131096 (2021).
[70] K. P. R. Nair, S. Herbers, , H. V. L. Nguyen, and J.-U. Grabow, Spectrochem. Acta. A **242**, 118709 (2020).
[71] M. Tudorie, I. Kleiner, M. Jahn, J.-U. Grabow, M. Goubet, and O. Pirali, J. Phys. Chem. A **117**, 1363 (2013).
[72] K. P. R. Nair, S. Herbers, J.-U. Grabow, and A. Lesarri, J. Mol. Spectrosc. **361**, 1 (2019).
[73] C. Thomsen, H. Dreizler, Z. Naturforsch. **56a**, 635 (2001).
[74] T. Bruhn and H. Mäder, J. Mol. Spectrosc. **200**, 151 (2000).
[75] A. Hellweg, C. Hättig, I. Merke, and W. Stahl, J. Chem. Phys. **124**, 204305 (2006).
[76] A. J. Shirar, D. S. Wilcox, K. M. Hotopp, G. L. Storck, I. Kleiner, and B. C. Dian, J. Phys. Chem. A **114**, 12187 (2010).
[77] A. Roucou, I. Kleiner, M. Goubet, S. Bteich, G. Mouret, R. Bocquet, F. Hindle, W. L. Meerts, and A. Cuisset, ChemPhysChem **19**, 1056 (2018).
[78] R. G. Bird and D. W. Pratt, J. Mol. Spectrosc. **266**, 81 (2011).
[79] W. Jäger, Microwave study of atmospheric oxidation and product *m*-toluic acid and its monohydrate, http://hdl.handle.net/2142/97117.